

Measurement-induced phase transition in periodically driven free-fermionic systems

Pallabi Chatterjee^{1,*} and Ranjan Modak^{1,†}

¹*Department of Physics, Indian Institute of Technology Tirupati, Tirupati 517619, India*

It is well known that continuous monitoring of a free-fermionic system leads to a steady state entanglement transition from a logarithmically entangled critical to the area law phase. While unitary evolution tends to grow the entanglement, continuous monitoring opposes this growth and results in the pinning of the wavefunction trajectories to the eigenstate of the measurement operators. In this work, we study the fate of this measurement-induced phase transition in a periodically driven free-fermionic quantum system, where the hopping amplitude is varied periodically in time. We show, in the high-frequency limit, that a renormalization group analysis of the non-Hermitian quantum sine-Gordon model [as proposed in Phys. Rev. X 11, 041004 (2021)] reveals a gapless critical phase with logarithmic entanglement entropy growth and a gapped area-law phase, separated by a Berezinskii-Kosterlitz-Thouless (BKT) transition, which is in excellent agreement with our numerical results. Further, the numerical evidence suggests that such BKT transition also prevails in the low-frequency regime, and decreasing frequency tends to favor the critical phase. Strikingly, we also find that if the hopping amplitude is varied completely symmetrically around zero in the form of square-pulse and sinusoidal drive, the BKT transition is absent in the thermodynamic limit, and the system always favors the area-law phase, independent of the frequency regime.

I. INTRODUCTION

Understanding the entanglement properties of quantum many-body systems has become a key focus of research, particularly in relation to different phases of matter and the transitions between them, as well as identifying quantum chaos at the many-body level^{1–9}. Thanks to recent progress on the direct measurement of entanglement dynamics with cold atoms and trapped ions, a key question of how entanglement spreads in out-of-equilibrium many-body systems brought lots of attention in the last decade^{10,11}. Entanglement entropy, a quantifier of quantum correlations between subsystems, exhibits distinct scaling behaviors that provide insight into the nature of the underlying phase. For example, in gapped quantum system, the ground state entanglement entropy typically obeys an area law (scales with the boundary area of the subsystem); in contrast, in one-dimensional critical systems, where long-range correlations are prevalent, it follows a logarithmic scaling with subsystem size, reflecting the scale-invariant nature of these systems at criticality^{12–14}. On the other hand, under unitary evolution, usually for clean short-ranged systems, the entanglement growth is algebraic in time before saturating to a value that scales linearly with the subsystem size, following a volume law^{13,15–17}. However, introducing disorder into systems changes the entanglement behavior drastically. In a closed, non-interacting quantum system, even small amounts of disorder—whether in one dimension or two—can prevent the thermalization of single-particle states, leading to a phenomenon known as Anderson localization¹⁸. Furthermore, when interactions are introduced into these disordered systems, the many-body localized (MBL) phase emerges^{19–26}. In the MBL phase, entanglement grows logarithmically over time, despite the absence of energy transport^{27–29}, in stark contrast to thermal systems, where entanglement growth is typically linear³⁰. Moreover, the typical eigenstate en-

tanglement entropy behaves quite differently in the thermal (ergodic) phase, which follows volume law scaling, compared to the non-ergodic MBL phase, where the scaling follows an area law³¹. Studies of the fate of MBL are not limited to closed systems; there are several interesting results reported where the system is coupled to a bath^{32–38}.

Another class of entanglement phase transitions arises from the continuous monitoring of quantum systems. The stochastic Schrödinger equation typically governs these open quantum dynamics, and averaging over different realizations of the states leads to the well-known Lindblad master equation dynamics³⁹. Since entanglement entropy is a nonlinear function of the state, calculating it for each trajectory separately and then averaging reveals a phase transition. In contrast, any linear function of the state is featureless and does not exhibit such transitions. Several studies have explored these entanglement phase transitions in both interacting and non-interacting systems, considering clean as well as disordered systems with long-range and short-range hopping, using both Lindblad jump operators and quantum state diffusion approaches^{40–47}. Continuously monitored open systems display competition between unitary evolution, which drives entanglement growth, and measurements, which tend to localize the wavefunction by collapsing it into eigenstates of the measurement operators. As a result, these systems undergo a measurement-induced phase transition as a function of measurement strength, which also has been reported recently in experiments⁴⁸. It has been shown that, in both clean and disordered free-fermionic systems, there is an entanglement phase transition from a critical to an area law phase as the strength of continuous measurements is tuned. This transition falls into the Berezinskii-Kosterlitz-Thouless universality class^{40–42}, a result that is also supported by a theoretical study in which the dynamics of a continuously monitored free fermionic system were described by an effective non-

Hermitian sine-Gordon model⁴⁹. There are recent theoretical studies of a monitored chain of a system of size L of Majorana fermions, which shows $(\ln L)^2$ behavior in the critical phase⁵⁰. However, it is important to point out that the stability of the critical phase in a one-dimension free-fermionic system under random projective measurements has been questioned recently, and it has been argued in the thermodynamic limit, for any finite measurement strength, only the area-law phase will survive⁵¹. On the other hand, in the case of interacting systems, a transition from a volume law to an area law has been observed^{45,46,52}. Furthermore, the role of measurements in localizing quantum states in nonunitary quantum circuits has also attracted significant interest⁵³⁻⁷⁰. Some of these studies have also been extended in dimension $D > 1$ ^{71,72} and a semi-classical limit of such transition has also been introduced recently⁷³. In contrast to disorder-induced localization observed in the Anderson-localized or MBL phase, the measurement-induced localization is governed by a completely different mechanism and driven by quantum measurements and measurement strength.

In parallel, in the last few decades, periodically driven (Floquet) quantum systems have emerged as a powerful framework for studying non-equilibrium phases of matter⁷⁴⁻⁷⁹. Floquet systems are known to exhibit exotic phases, such as discrete-time crystals⁸⁰⁻⁸² and Floquet topological insulators⁸³⁻⁸⁷. The fate of many-body localization (MBL) in the presence of a periodic drive has also been studied^{88,89}. While it has been demonstrated that Floquet systems can stabilize or even induce new phases, it remains an open question how continuous monitoring affects these driven systems and whether the introduction of periodic drive can significantly alter the dynamics of a continuously monitored system, either enhancing or suppressing the effects of measurements. The effect of time-dependent Hamiltonian has been studied within the Lindblad master equation formalism^{90,91}, but the effect of periodic drive on a continuously monitored open quantum system, particularly in terms of trajectory-averaged entanglement entropy, remains unexplored. In our study, we investigate such cases, and our main finding is that periodically driven non-interacting systems also go through BKT transition. In general, for a given drive protocol, the low-frequency regime favors the critical phase more, implying that the critical measurement strength (transition point) increases with the time period. We also find that the effective dynamics of continuously monitored free-fermionic systems with no drive can mimic the high-frequency limit. Moreover, the symmetric drive of the hopping amplitude about a zero mean is special, such a system always favors the area-law phase in the thermodynamic limit, independent of the frequency regime, in contrast to what has been observed in the case of disorder-induced scenario⁷⁵. We summarize our set-up and main results in the form of a schematic in Fig. 1.

This manuscript is structured as follows. In Sec. II, we describe our system and protocols. Then, to build the intuitions about our systems, we focus on a 2×2 toy

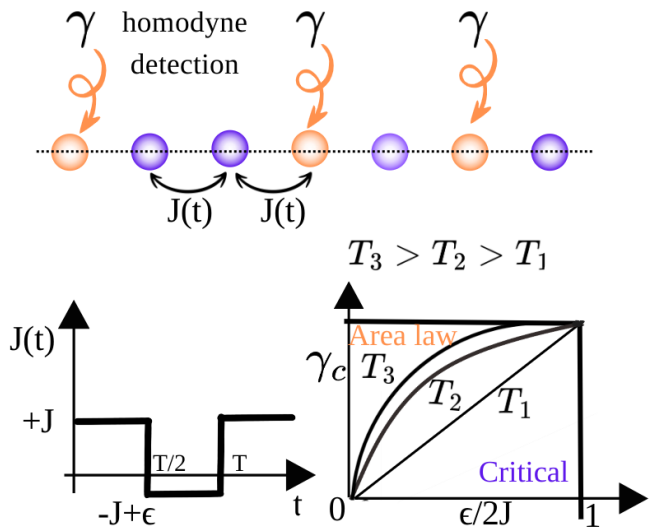


FIG. 1. Schematic of our protocol, where a free-fermionic lattice is continuously monitored, and the hopping amplitude $J(t)$ is periodically varied. Phase diagrams for the critical and area-law phases are shown for different time periods, and $\epsilon/2J = 1$ corresponds to no drive result.

model in Sec. III. Section. IV is dedicated to the many-body systems, which consists of the analytical prediction for high-frequency limit in sec. IV A, as well as the numerical results in sec. IV B. Section. IV C concentrates on a particular drive protocol that is symmetric around zero means. Finally, we summarize our results in sec. V.

II. MODEL AND METHODOLOGY

We consider spinless fermions in a periodic tight-binding lattice of the length L where the hopping amplitude changes periodically with time, and the system is continuously monitored. The Hamiltonian of this system is given by:

$$H(t) = J(t) \sum_{i=1}^L \hat{c}_i^\dagger \hat{c}_{i+1} + h.c., \quad (1)$$

where, \hat{c}_i^\dagger and \hat{c}_i are real-space fermionic creation and annihilation operators respectively. We study the effect of two different kinds of driving with the time period (frequency) T ($\omega = 1/T$): one is square pulse drive, where $J(t) = +J$ ($-J + \epsilon$) for $0 \leq t < T/2$ ($T/2 \leq t < T$), with ϵ varying between 0 to $2J$ (see Fig. 1); the other is the sinusoidal drive where $J(t) = J \sin(2\pi t/T)$. Note that in the limit $\epsilon = 0$, the mean of $J(t)$ is 0 over a time period. We examine this limit separately in this manuscript. We primarily present the results for the square pulse in the subsequent sections of the manuscript; only at the end, in Sec. IV C, some results for the sinusoidal drive are presented. For all our numerical calculations, we choose

$J = 1/2$. The time evolution of the state can be described using the stochastic Schrodinger equation as

$$d|\psi(t)\rangle = -iH(t)dt|\psi(t)\rangle - \frac{\gamma dt}{2} \sum_i (\hat{n}_i - \langle \hat{n}_i \rangle)^2 |\psi(t)\rangle + \sum_i (\hat{n}_i - \langle \hat{n}_i \rangle) dW_i^t |\psi(t)\rangle. \quad (2)$$

The above equation describes the continuous monitoring of the particle number $\hat{n}_i = \hat{c}_i^\dagger \hat{c}_i$ on each site, with measurement strength γ ⁴². dW_i s are taken from uncorrelated normal distributions having mean 0 and variance γdt , which implies, $\overline{dW_{i,t}} = 0$ and $\overline{dW_{i,t} dW_{j,t'}} = \gamma dt \delta_{i,j} \delta(t-t')$. For our model and protocols, the total number of particles $N = \sum_i \langle \hat{n}_i \rangle$ remain conserved in the entire time evolution process; hence, if we start with an initial state with a particular filling at $t = 0$, for any time $t > 0$, the filling fraction remains the same. In our work, we have fixed the filling fraction $N/L = 1/2$ for all many-body calculations. Also, note that the last two terms in Eq. (2) describe the contribution from the continuous measurement process and can be realized by homodyne detection in quantum optics^{92,93}.

In order to solve Eq. (2), one needs to perform Trotterization and can write,

$$|\psi(t+dt)\rangle = \mathcal{N} e^{\mathcal{M}} e^{-iH(t)dt} |\psi(t)\rangle, \quad (3)$$

where, $\mathcal{M} = \sum_i [dW_i^t + (2\langle \hat{n}_i \rangle - 1)\gamma dt] \hat{n}_i$, and \mathcal{N} is the normalization constant. Any pure Gaussian state can be represented as,

$$|\psi\rangle = \prod_{i=1}^N \left(\sum_{j=1}^L U_{ji} \hat{c}_j^\dagger \right) |0\rangle. \quad (4)$$

As $|\psi(t)\rangle$ evolves according to Eq. (3), and it preserves the Gaussianity of the state, hence; it is straight forward to show that the U evolves as,

$$U(t+dt) = e^{\mathcal{M}} e^{-iH(t)dt} U(t), \quad (5)$$

where $H(t) = J(t) \sum_{i=1}^L (\hat{c}_i^\dagger \hat{c}_{i+1} + h.c.)$ is the single particle Hamiltonian and $M_{ij} = \delta_{i,j} [dW_i^t + (2\langle \hat{n}_i \rangle - 1)\gamma dt]$. Under this non-Hermitian evolution, we need to properly normalize the wavefunction in each step, which can be done using the QR decomposition of the U matrix in each step as $U(t+dt) = QR$, and we set the new U as Q . Note that U is an $L \times N$ matrix, follows $U^\dagger U = \mathbb{I}_{N \times N}$. On the other hand, the correlation matrix D can be defined as $D_{ij} = \langle \hat{c}_i^\dagger \hat{c}_j \rangle = [UU^\dagger]_{ij}$. For our many-body calculations, we choose dW_i s from different random realizations, compute the nonlinear function of states, e.g., entanglement entropy using the correlation matrix for each realization separately, and finally average over different realizations (we ensure the convergence of our results by varying the realization number). On the other hand, the evolution of the average state will be governed by the Lindblad equation⁴².

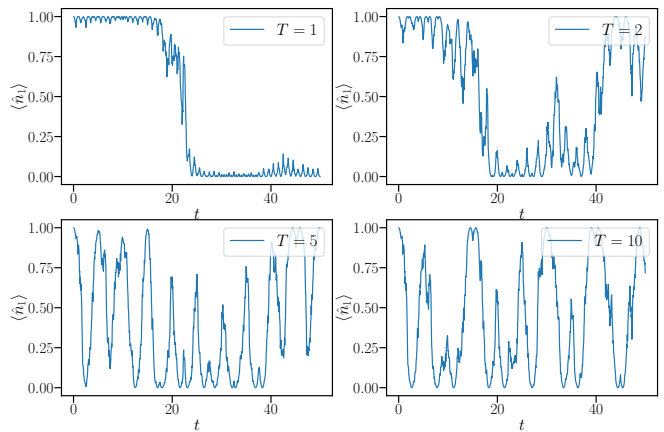


FIG. 2. The variation of the expectation value of fermionic occupancy, $\langle \hat{n}_1 \rangle$, at site 1 as a function of time t for a typical single trajectory in a 2×2 periodically driven toy model, for different values of T and with $\epsilon = 0$ fixed.

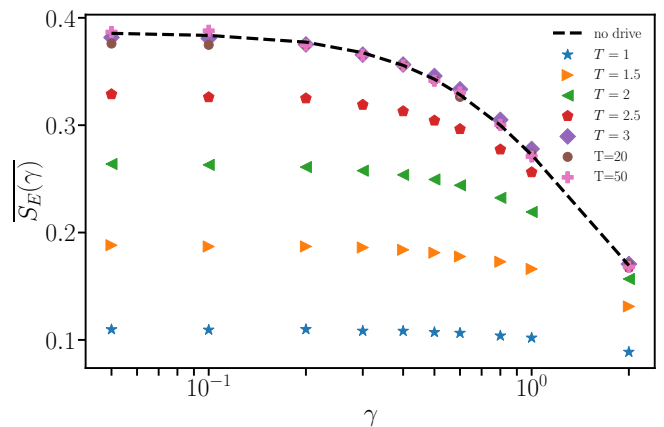


FIG. 3. $\overline{S_E(\gamma)}$ vs. γ plots for different driving periods for $\epsilon = 0$ at steady state. The black dashed line corresponds to no-drive results with $J(t) = J = 1/2$.

III. 2×2 TOY MODEL

In this section, we study a periodically driven, continuously monitored 2×2 system to gain insight into the effect of driving on the system under a square pulse driving protocol. We use the same Hamiltonian as in Eq. 1 and the same protocol as described in Sec. II but limit ourselves to two sites and one particle. In this system, the Hilbert space is spanned by the basis states $|01\rangle$ and $|10\rangle$, which are also the eigenstates of the measurement operators \hat{n}_1 and \hat{n}_2 . In Fig. 2, we plot the expectation value of the occupancy $\langle \hat{n}_1 \rangle$ at site 1 for a typical single trajectory as a function of time, for different driving periods T , but for the fixed $\gamma = 0.1$ and $\epsilon = 0$. For very small T , i.e., in the high-frequency regime, $\langle \hat{n}_1 \rangle$ remains mostly at either 0 or 1, indicating that the particle is pinned or localized in the eigenstates of the measurement operator or at the dark states, even for a small measure-

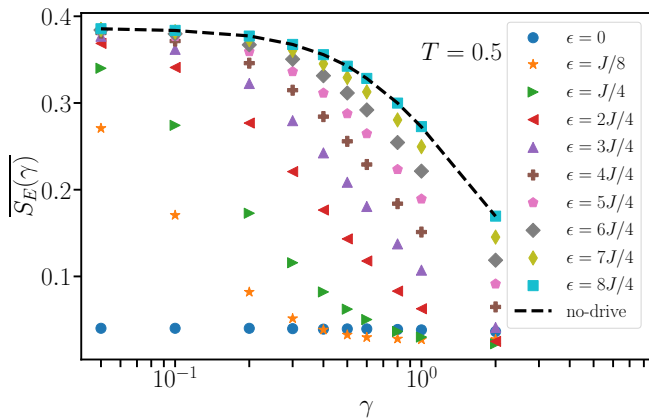


FIG. 4. $\overline{S_E(\gamma)}$ vs. γ plots for different ϵ values, for $T = 0.5$ at steady state. In the limit $\epsilon = 2J$, we get back the no-drive ($J(t) = J = 1/2$) result, which is represented by the black dashed line.

ment strength $\gamma = 0.1$. In contrast, as we increase T , the particle becomes depinned from the dark states.

To quantify this behavior more systematically, we define a measure,

$$S_E(\gamma) = -\langle \hat{n}_1 \rangle \ln \langle \hat{n}_1 \rangle - \langle \hat{n}_2 \rangle \ln \langle \hat{n}_2 \rangle. \quad (6)$$

$S_E(\gamma)$ is averaged over different random trajectories, followed by a long-time average, which we denote as $\overline{S_E(\gamma)}$. In the localized or pinned phase, where both $\langle \hat{n}_1 \rangle$ and $\langle \hat{n}_2 \rangle$ remain at 0 or 1 most of the time, the steady-state value of $\overline{S_E(\gamma)}$ tends to zero. In contrast, in the delocalized phase, this value becomes significantly greater than zero. In Fig. 3, we plot the steady-state value of $\overline{S_E(\gamma)}$ as a function of γ for different driving periods. For a very small driving period, $T = 1$, $\overline{S_E(\gamma)}$ is almost zero for all γ . As we increase T , the steady-state value $\overline{S_E(\gamma)}$ gradually increases at least for small γ . This behavior indicates a potential transition from depinning to pinning as γ increases, particularly for large T . Interestingly, for $T \gtrsim 2.5$, the steady-state value $\overline{S_E(\gamma)}$ stabilizes and shows almost negligible change upon increasing T further. Moreover, $T \gtrsim 2.5$ data is almost indistinguishable from the no-drive results. This gives us a hint that large T promotes depinning, and also, for $\epsilon = 0$, the large T limit may resemble a no-drive scenario even for many-body systems.

While Fig. 3 focuses on the case with $\epsilon = 0$, we now examine the dependence of $\overline{S_E(\gamma)}$ on ϵ in the high-frequency regime with $T = 0.5$. Figure 4 shows that for $\epsilon = 0$, $\overline{S_E(\gamma)}$ remains nearly zero for all γ , as also observed in Fig. 3. As ϵ increases, we observe a typical increase in $\overline{S_E(\gamma)}$. However, with further increases in γ , $\overline{S_E(\gamma)}$ approaches zero even for finite ϵ , indicating a transition from depinning to pinning. From Fig. 4, it is also evident that the decay of $\overline{S_E(\gamma)}$ to zero occurs more rapidly for smaller ϵ compared to larger ϵ . This suggests, indirectly, that the critical measurement strength γ_c (if a

measurement-induced transition exists) may decrease as ϵ decreases, favoring more the localized phase. In the following sections, we will now focus on the many-body Hamiltonian.

IV. MANY-BODY SYSTEM

In this section, we focus on the periodically driven many-body system described by the Hamiltonian in Eq. (1), which is continuously monitored. We initialize the system in a Néel state $|\psi_0\rangle = |1010\dots\dots 1010\rangle$ at time $t = 0$ and let the system evolve according to Eq. (2). In the absence of a drive, such a system undergoes a transition from the critical to the localized phase (depinning to pinning transition), which has been previously characterized using the scaling of entanglement entropy with system size^{50,94,95}. In our work, we also use entanglement entropy as a diagnostic tool.

The entanglement between subsystem A of length l_A and the rest of the system is measured by the von Neumann entanglement entropy, which is defined as $S = -\text{tr}(\rho_A \ln \rho_A)$ ⁹⁶, where the reduced density matrix ρ_A is obtained by tracing over the degrees of freedom of the rest of the system (which we identify as B), i.e., $\rho_A = \text{tr}_B |\psi(t)\rangle\langle\psi(t)|$. Even in the continuously monitored driven system we are interested in, the evolution generators are quadratic, preserving the Gaussianity of the quantum trajectories. Hence, the entanglement entropy S can be easily calculated using the eigenvalues λ_i of the correlation matrix $D_{ij} = \langle \hat{c}_i^\dagger \hat{c}_j \rangle$ as^{2,97,98},

$$S(l_A, L) = -\sum_{i=1}^{l_A} [\lambda_i \ln \lambda_i + (1 - \lambda_i) \ln(1 - \lambda_i)].$$

In our calculation, we take $l_A = L/2$, where L is the total system size. Thus, the eigenvalues of the correlation matrix D_{ij} are computed by restricting the indices up to $L/2$. After calculating the entanglement entropy for each trajectory, we average over different realizations, which we denote as \overline{S} . In the subsequent sections, we study the behavior of \overline{S} in great detail for different frequency regimes.

A. High-frequency regime: Analytical prediction

It has been proposed recently that in the absence of the driving, the long-time dynamics of the continuously monitored fermionic Hamiltonian given by Eq. (1) could be theoretically described by an effective bosonized non-Hermitian sine-Gordon model⁴⁹,

$$H_{eff} = \frac{vJ}{2\pi} \int_x \left[(\partial_x \hat{\phi}_x)^2 + \left(1 - \frac{2i\gamma}{vJ\pi}\right) (\partial_x \hat{\phi}_x)^2 \right] + i\lambda \int_x \left[\cos(\sqrt{8}\hat{\phi}_x - 1) \right]. \quad (7)$$

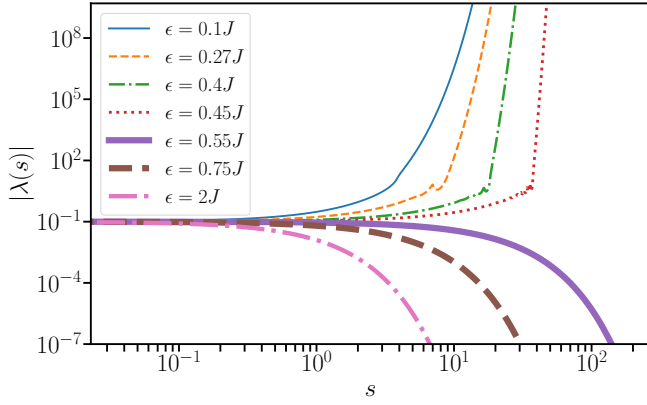


FIG. 5. Flow of λ for different ϵ values, with same initial condition $|\lambda| = 0.1$ and $|K(\epsilon = 2J)| = 1.42\pi$. For $\epsilon = 2J$, the flow of λ is towards the Gaussian fixed point, which suggests a critical phase; on decreasing ϵ , the flow of λ approaches the strong coupling fixed point, which suggests area-law entanglement phase. In our calculation, we take $A = 1$.

Here, $v = \partial_k E(k)|_{k=k_F}$, $E(k) = 2 \cos k$ for free theory and k_F is fermi momentum, $\hat{\phi}_x$ is the bosonic field operator with its conjugate field $\hat{\theta}_x$ obeying the commutation relation $[\partial_x \hat{\theta}_x, \hat{\phi}_{x'}] = -i\pi\delta(x - x')$, and $\lambda = \gamma m^2$, where m is $O(1)$, depends on normal ordering prescription. It has been shown recently that in a long-time steady state, the system comes to a dark state, which is defined as the zero energy eigenstate of the H_{eff} , i.e., $H_{eff}|\psi_D\rangle = 0$ (or equivalently can be identified as an eigenstate of the evolution operator $U(T) = e^{-iH_{eff}T}$ with eigenvalues 1, i.e., $U(T)|\psi_D\rangle = |\psi_D\rangle$). The steady-state entanglement entropy can be obtained from^{13,99},

$$S(l_A) = \frac{1}{3} \langle \psi_D | \hat{\phi}_x \hat{\phi}_{x+l_A} | \psi_D \rangle. \quad (8)$$

In the case of the square pulse driving protocol (as discussed in Sec. II), in a similar spirit, one can write down the effective Floquet evolution operator in terms of the non-Hermitian sine-Gordon Hamiltonian as

$$U_F(T) = e^{-iH_{eff}^+ T} = e^{-iH_{eff}^- T/2} e^{-iH_{eff}^+ T/2}, \quad (9)$$

where,

$$H_{eff}^+ = \frac{Jv}{2\pi} \int_x \left[(\partial_x \hat{\theta}_x)^2 + \left(1 - \frac{2i\gamma}{Jv\pi}\right) (\partial_x \hat{\phi}_x)^2 \right] + i\lambda \int_x \left[\cos(\sqrt{8}\hat{\phi}_x - 1) \right].$$

and

$$H_{eff}^- = \frac{(-J + \epsilon)v}{2\pi} \int_x \left[(\partial_x \hat{\theta}_x)^2 + \left(1 - \frac{2i\gamma}{(-J + \epsilon)v\pi}\right) (\partial_x \hat{\phi}_x)^2 \right] + i\lambda \int_x \left[\cos(\sqrt{8}\hat{\phi}_x - 1) \right],$$

and in the high-frequency limit, the effective Floquet Hamiltonian H_{eff}^F can be calculated using Magnus expansion as¹⁰⁰,

$$H_{eff}^F = \frac{1}{2}(H_{eff}^- + H_{eff}^+) - \frac{iT}{4}[H_{eff}^-, H_{eff}^+] + O(T^2). \quad (10)$$

In the extremely high-frequency limit ($T \ll 1$), H_{eff}^F can be approximated by the 1st term in the Magnus expansion as,

$$H_{eff}^F \simeq \left[\frac{v\epsilon}{4\pi} \int_x \left[(\partial_x \hat{\theta}_x)^2 + \eta^2 (\partial_x \hat{\phi}_x)^2 \right] + i\lambda \int_x \left[\cos(\sqrt{8}\hat{\phi}_x - 1) \right] \right], \quad (11)$$

where $\eta^2 = 1 - \frac{4i\gamma}{\epsilon\pi v}$. Hence, one would expect that in such a high-frequency limit, the steady state of the driven continuously monitored system, as discussed in Sec. II, can be described by the dark state of the non-Hermitian sine-Gordon Hamiltonian Eq. (11) and steady state entanglement entropy can be obtained using Eq. (8), $|\psi_D\rangle$ correspond to the zero energy eigenstate of the Hamiltonian Eq. (11). Moreover, this also suggests that the entanglement dynamics in the low-frequency limit can effectively be mimicked by the continuously monitored no-drive dynamics of tight-binding Hamiltonian with effective hopping amplitude $J_{eff} = \epsilon/2$. It also automatically implies if in the no drive case, i.e., $\epsilon = 2J$, the transition point is at $\gamma_c = \gamma_0$, for $\epsilon < 2J$ (the drive is introduced), the transition point will be $\gamma_c = \epsilon\gamma_0/2J$, decays to zero linearly with decreasing ϵ .

In the case of the $\epsilon > 0$ and $\lambda = 0$, the Hamiltonian Eq. (11) has a Gaussian fixed point, which implies the logarithmic scaling of the entanglement entropy with subsystem size will prevail⁴⁹, i.e.,

$$S = \frac{1}{3} C(\gamma) \ln(l_A), \quad (12)$$

where $C(\gamma)$ is referred to as the effective central charge. We refer to this phase as a critical phase. One needs to find out renormalization flow equations to study the effect of the nonlinearity λ and investigate the fate of the Gaussian fixed point. The Hamiltonian Eq. (11) can be brought in its action form using complex wick rotation $(x, t) \rightarrow (\tilde{\epsilon}^{1/2}\tilde{\eta}^{1/2}x, i\tilde{\epsilon}^{-1/2}\tilde{\eta}^{-1/2}t)$, and the action \mathcal{F} reads as,

$$\mathcal{F} = \int_X \frac{K}{16\pi} (\nabla \hat{\phi}_X)^2 + i\lambda \cos(\hat{\phi}_X), \quad (13)$$

where $(\nabla \hat{\phi}_X)^2 = (\partial_x \hat{\phi}_X)^2 + (\partial_t \hat{\phi}_X)^2$, $X \in (x, t)$, $\tilde{\epsilon} = v\epsilon/2\pi$, and $K^2 = \eta^2$. We use a similar renormalization group (RG) prescription as discussed in Ref.^{49,101}, first, decompose the fields into short-range modes that correspond to momentum $\frac{\Lambda}{\zeta} < |k| < \Lambda$ and the long-range modes that correspond to $|k| < \frac{\Lambda}{\zeta}$ (Λ is a short-distance

cutoff, and $\zeta = e^s$, and s is the rescaling parameter controlling the renormalization group flow), and finally, integrate out the short-range modes. One can write down renormalization group flow equations perturbatively in λ as (note these equations are identical as obtained in Ref.⁴⁹),

$$\begin{aligned}\partial_s \lambda &= \left(2 - \frac{8\pi}{K}\right)\lambda \\ \partial_s K &= -\lambda^2 A,\end{aligned}\quad (14)$$

where A is a positive number of order $O(1)$ determined by the propagator of the Gaussian theory. If increasing the RG iteration step λ grows, it signifies that the non-linearity is relevant perturbation; on the other hand, if λ decays, that will make the perturbation irrelevant, and the physics will still be governed by the Gaussian fixed point, implies the survival of the critical phase. In Fig. 5 we numerically solve the Eq. (14) with initial condition $|\lambda(s=0)| = 0.1$ and $K(s=0, \epsilon) = \sqrt{\frac{2J}{\epsilon} K^2(s=0, \epsilon=2J) + 1 - \frac{2J}{\epsilon}}$, with $|K(s=0, \epsilon=2J)| = 1.42\pi$. We choose the initial condition in such a way that for $\epsilon = 2J$ (no-drive scenario), λ decreases with increasing s , signifies RG flow towards the Gaussian fixed point, implying the critical phase. The question we ask is if we change ϵ (indirect way to introduce drive), how λ will change with RG steps? We find that for $\epsilon = 0.75J$ and $0.55J$, it decreases with increasing s . On the other hand, on decreasing ϵ further, the λ starts growing with s , which makes the non-linear λ term relevant. It signifies that physics is no longer governed by the Gaussian fixed point; instead, it is governed by a strong coupling fixed point, which is responsible for the area-law entanglement phase. This study also shows that decreasing ϵ promotes the area-law entanglement phase, and if one starts with an initial condition such that the no-drive scenario shows a critical phase, with decreasing ϵ one should be able to probe the critical-area law phase transition⁴⁰.

Next, we try to understand the effect of ϵ on the critical phase, more precisely, how the correlation or entanglement entropy depends on our drive protocol. We just focus on the $\lambda = 0$ limit of the Hamiltonian (11), which can be expressed in the momentum space representation as,

$$H_{eff}^F(\lambda=0) = \frac{v\epsilon}{4\pi} \int_q q^2 \left[\hat{\theta}_q \hat{\theta}_{-q} + \hat{\eta}_q^2 \hat{\phi}_q \hat{\phi}_{-q} \right].$$

It has been argued that this Hamiltonian has a unique dark state⁴⁹, and the correlation function in this dark state is given by,

$$\langle \psi_D | \hat{\phi}_q \hat{\phi}_{-q} | \psi_D \rangle = \frac{v^{3/2} \sqrt{\pi\epsilon}}{8\gamma|q|} \sqrt{2\sqrt{16\gamma^2 + (v\pi\epsilon)^2} - 2v\pi\epsilon}.$$

It is straightforward to check that for a fixed non-zero γ , in the limit $\epsilon \rightarrow 0$, this correlation tends to zero, and the effective central charge $C(\gamma)$ (note that the leading

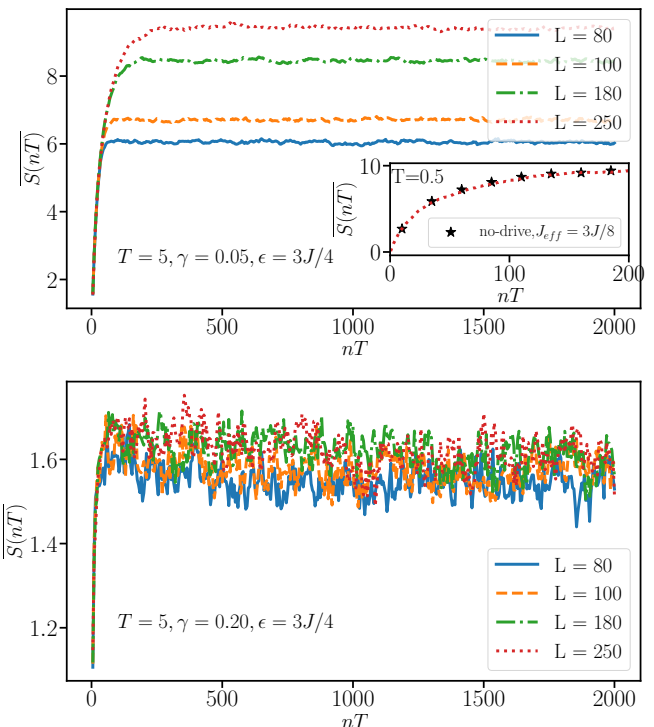


FIG. 6. Stroboscopic growth of trajectory averaged entanglement entropy for $\gamma = 0.05$ (upper panel) and $\gamma = 0.20$ (lower panel). All plots are for $\epsilon = 3J/4$ and $T = 5$. The upper panel inset shows that in the high-frequency regime $T = 0.5$, the numerical results are in agreement with no-drive results for $J_{eff} = 3J/8$. Inset data is for $\gamma = 0.05$ and $N = 250$.

order term in the entanglement entropy $S = \frac{C(\gamma)}{3} \ln l_A$) will also approach zero as $\sqrt{\frac{\epsilon}{\gamma}}$. This implies that in the case of $\epsilon = 0$, for any finite γ , one would expect to observe the area-law phase. In a nutshell, we make three main predictions about the high-frequency limit drive: 1) the entanglement dynamics can be mimicked by the dynamics of no-drive continuously monitored free-fermionic chain with the hopping amplitude $J_{eff} = \epsilon/2$, 2) If one starts in critical-phase in the no-drive regime, i.e. $\epsilon = 2J$, with decreasing ϵ , one can be able to probe critical to area-law phase transition, 3) $\epsilon = 0$ limit will not display entanglement transition, it will always show the area-law entanglement for any non-zero finite measurement strength, 4) the transition point γ_c is expected to decay to zero linearly with decreasing ϵ . Next, we will try to test our analytical prediction using numerical simulation on a finite-size tight-binding lattice.

B. Numerical results

In this section, we perform a numerical experiment on a finite-size lattice with periodic boundary conditions using the methodology described in Sec. II. First, we study the time evolution of the entanglement entropy, i.e., av-

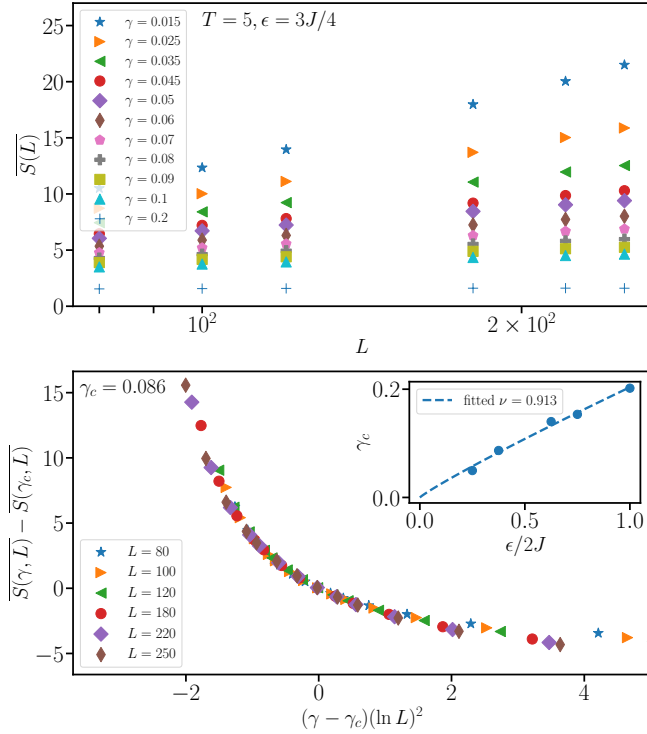


FIG. 7. Upper Panel: System size scaling of steady state trajectory averaged entanglement entropy $\bar{S}(L)$ for different γ . Lower Panel: Data collapse of entanglement entropy for different L and γ assuming the BKT type scaling ansatz with critical measurement strength $\gamma_c = 0.086$. The results are for $T = 5$ and $\epsilon = 3J/4$. The inset in the lower panel shows the variation of the γ_c (obtained from the data-collapse) for different ϵ .

eraged over many different trajectories, starting from the initial zero entanglement product state for different values of ϵ and measurement strengths γ , for $T = 5$. Figure. 6 shows the dynamics of $\overline{S(nT)}$ for $\epsilon = 3J/4$. The upper panel shows for $\gamma = 0.05$, the saturation value of the entanglement entropy increases with system size; on the other hand, the lower panel shows for $\gamma = 0.2$, the steady state value of the average entanglement entropy hardly changes with system size. This is a signature that, with increasing measurement strength, an entanglement transition may occur, where for small values of γ , the steady-state entanglement increases with L , and for large γ , it does not scale with L . The inset of the upper panel shows the entanglement dynamics in high-frequency regime $T = 0.5$ for $\gamma = 0.05$ and $L = 250$ (red-dotted line). As predicted in the previous section, we find that, indeed, for $T = 0.5$, the entanglement dynamics can be mimicked by the continuously monitored no-drive scenario in a tight-binding lattice with an effective hopping strength $J_{eff} = \epsilon/2$, which is denoted by points in the inset figure. We further check the system size scaling of steady-state entanglement entropy for $\epsilon = 3J/4$ in Fig. 7 (upper panel) for different γ values. It shows clear evidence of a logarithmic-area law entan-

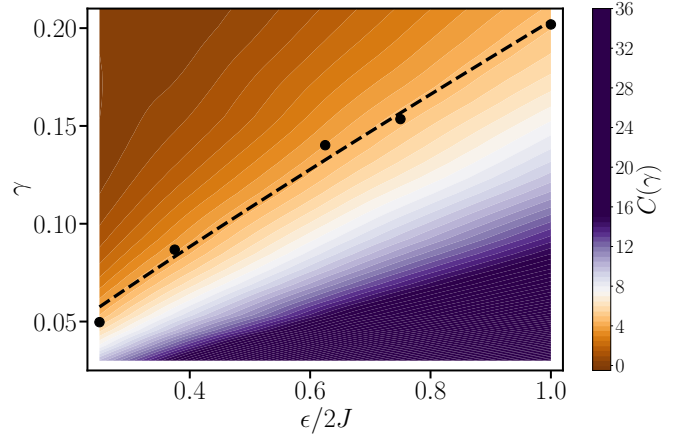


FIG. 8. Color variation corresponds to the different values of the effective central charge $C(\gamma)$ for $T = 5$. Black Dots represent γ_c , and the dashed line is the best-fit line, identifying the phase transition.

glement phase transition. To re-confirm that for small γ , the scaling is logarithmic (not volume law), we also perform an F-test (see Appendix. C). It has been shown recently that in the absence of driving, the measurement-induced critical to area-law phase transition with increasing γ belongs to the BKT universality class^{40,41}. The system size dependence of the entanglement entropy in the BKT universality class obeys the following scaling form in the vicinity of the critical γ_c ¹⁰²,

$$\bar{S}(L/2, L, \gamma) - \bar{S}(L/2, L, \gamma_c) = F[(\gamma - \gamma_c)(\ln L)^2]. \quad (15)$$

Given that the steady entanglement entropy growth is logarithmic in a small γ regime, we also use the similar BKT scaling ansatz to obtain the critical γ_c values for different ϵ and different values of T . Figure. 7 (lower panel) shows the data collapse of steady state entanglement entropy for different L and γ , which confirms that the transition belongs to the BKT universality class and allows us to evaluate the critical γ_c . We use the cost function minimization technique to obtain the γ_c (see Appendix. B). Inset shows the critical γ_c values for different ϵ . Our results suggest the critical γ_c decreases with decreasing ϵ and approaches zero in the $\epsilon \rightarrow 0$ limit, as also predicted by our previous RG study for high-frequency limit. The best fit suggests $\gamma_c \sim (\epsilon/2J)^\nu$, where $\nu \simeq 0.91$, slightly smaller than 1. Note that $\nu = 1$ was predicted previously in sec. IV A for the high-frequency limit. Figure. 8 shows the contour plot of the effective central charge $C(\gamma)$ for different values of γ and ϵ , and dots correspond to the γ_c and the dashed line corresponds to the best-fit line. Also, important to point out, given our $T = 0.5$ data are almost indistinguishable from the no-drive data with $J_{eff} = \epsilon/2$, one will obtain $\nu = 1$ for $T = 0.5$. $\nu < 1$ for $T = 5$ also signifies that with increasing T , γ_c will increase for a given ϵ ; it will promote the critical phase more. Moreover, the data for $T = 5$ also suggests that for a symmetric drive with zero means, i.e.,

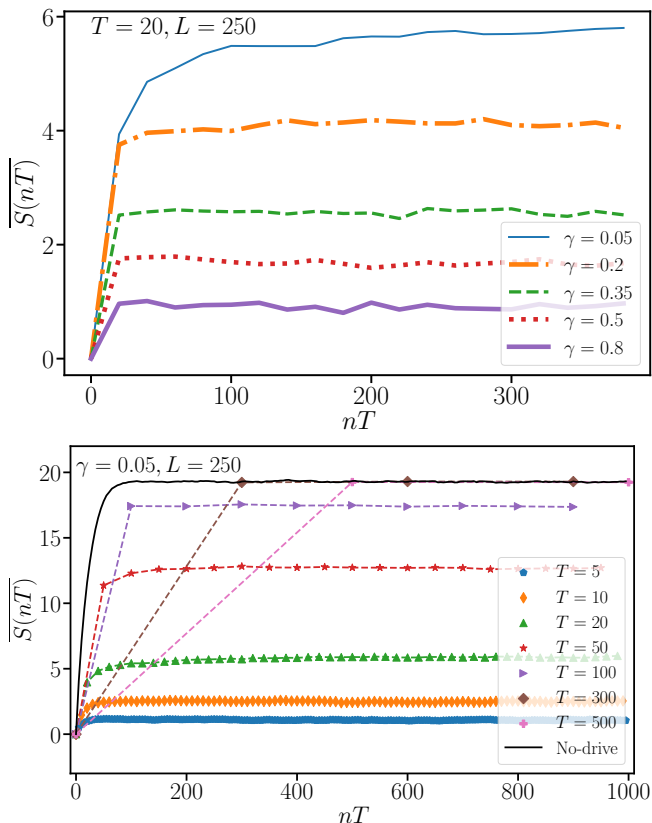


FIG. 9. Stroboscopic growth of trajectory averaged entanglement entropy for different T and γ . Upper panel: for $T = 20$ and varying γ , Lower panel: for $\gamma = 0.05$ and varying T . Plots are for system size $L = 250$ and $\epsilon = 0$.

for $\epsilon = 0$, $\gamma_c \rightarrow 0$, implies no transition, always area-law phase. Though our analytical results suggest the same for the high-frequency regime; it is not at all obvious that this phenomenon persists even for large T . Especially given that there are examples where disorder-induced localization-delocalization transition has been observed in the large T limit for symmetric drive mean around zero^{75,76}. Hence, in the next section, we investigate the $\epsilon = 0$ limit even more carefully.

C. Symmetric drive with zero mean: $\epsilon = 0$ limit

Square pulse drive: Here, we focus on the $\epsilon = 0$ limit. First, the time evolution of the entanglement entropy, i.e., averaged over many different trajectories, starting from the initial Neel state for different values of time period T and measurement strengths γ , is studied. We find that \overline{S} increases with time initially and then saturates to a steady state value. From Fig. 9 upper panel, we see, for a fixed driving period $T = 20$, if we increase the measurement strength γ , the steady state entanglement saturation value is decreased; similar to our previous results, the entanglement spread gets suppressed because

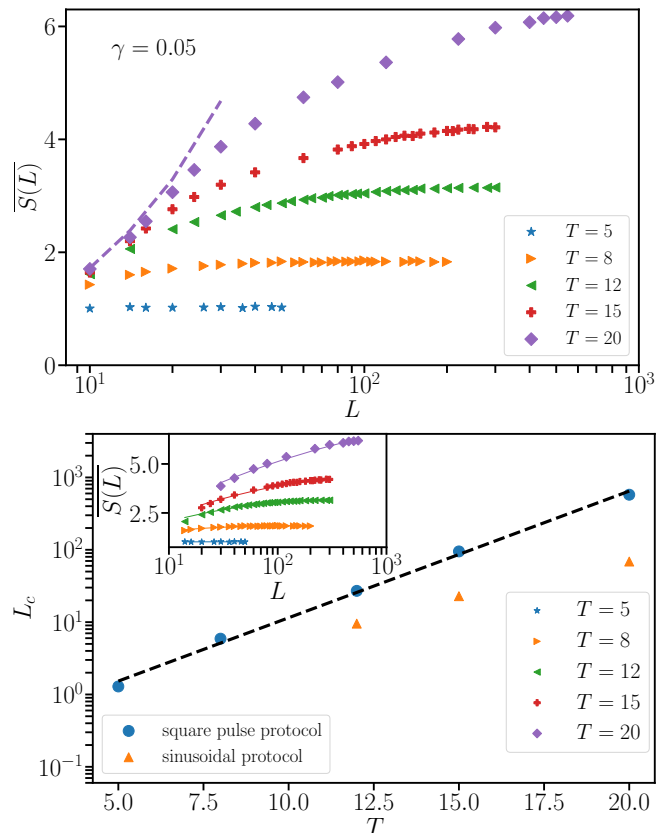


FIG. 10. Upper panel: Scaling of the steady state entanglement entropy with system size L for different T , but fixed $\gamma = 0.05$ and $\epsilon = 0$. Initially, it shows logarithmic growth with L and then tends to saturate. Dashed-line corresponds to no-drive $J = 1/2$ results for $\gamma = 0.05$. Lower panel: plot of L_c vs. T , L_c is estimated using Eq. (16), circles are for square pulse protocol, and triangles are for sinusoidal protocol. Inset shows the best fit of the entanglement entropy assuming the functional form given by Eq. (16) for square pulse protocol.

of increasing measurement strength. On the other hand, it is shown in the lower panel of Fig. 9 that, for a fixed measurement strength $\gamma = 0.05$, the entanglement saturation value increases with the increase of the driving time-period T . This suggests, in general, that the low driving frequency promotes the depinning of the particles, and the entanglement entropy saturation values approach the no-drive result with increasing T . We also noticed there is a critical driving period T_c , such that for $T > T_c$, the results are almost indistinguishable from those of the no-drive scenario. However, this T_c typically increases with L . The fact that $T > T_c$ resembles a no-drive situation has also been observed for our 2×2 Toy model previously.

Next, we immediately ask the following question: How does the steady-state entanglement entropy change with the subsystem size for different T ? The existence of a T_c for each L might be a tempting scenario to conjecture that in the very large T limit, $\epsilon = 0$ results should

resemble no-drive results and should display an entanglement transition. However, one needs to take the large T and large L limits carefully. The order of these two limits doesn't commute. If one takes a large T limit first, then any finite L (no matter how large it is), T_c has been achieved, and hence, one will observe no-drive results, i.e., the presence of the measurement-induced transition. On the other hand, the correct limit is to take the large L limit first, then increase the T . In that case, the outcome will be different, and we further try to argue that in this limit, there will be no transition.

Given for each L , a critical T_c exists, and if one chooses a reasonably large T , it will turn out to be a T_c for some system size $L = L_1$. Hence, for that particular T , till $L < L_1$, the saturation value will resemble the no-drive results, which implies it will show logarithmic scaling for $L < L_1$ for small γ , but for $L > L_1$, the steady entanglement data vs L will certainly show a bending because if $T < T_c$, the entanglement saturation value is smaller than the $T \geq T_c$ value. We precisely see that in Fig. 10 upper panel. We find for $\gamma = 0.05$ and $T = 5$, and 8, the steady state entanglement entropy is almost constant for all L , which suggests an area law scaling with the system size. On the other hand, as we increase T , we see an initial logarithmic scaling of entanglement entropy with system size till $L < L_1$, followed by bending trend, finally after a critical $L = L_c$, entanglement starts showing area law behavior. The dashed line corresponds to the no-drive results for $J = 1/2$ and $\gamma = 0.05$. Roughly, till $L \simeq 20$, this no-drive results resembles $T = 20$ data, beyond $L = 20$, the no-drive results keep increasing with L , while the $T = 20$ data starts bending (see appendix. A for $T = 100$ results). To estimate the L_c , we fit the steady entanglement entropy vs L data with a two parameters (S_{sat} and L_c) fitting function $f(L)$, i.e.,

$$f(L) = S_{sat} \tanh\left(\frac{\ln L}{\ln L_c}\right), \quad (16)$$

in the inset of Fig. 10 lower panel. In the limit $L \gg L_c$, $f(L) \rightarrow S_{sat}$, which is a constant suggesting area-law phase, on the other hand, for $L \ll L_c$, $f(L) \propto \log L$. We estimate L_c from the best fit and plot L_c vs T in Fig. 10 lower panel, which suggests an exponential growth of L_c with the driving period T . As an exercise, we estimate the fitting parameter L_c for $T = 100$ and $\gamma = 0.05$ from the exponential fit, which gives $L_c \simeq 10^{16}$. Hence, it is almost impossible to reach the accessible system size regime to see area law scaling for $T = 100$ (see Fig. 12 in Appendix A for details).

Sinusoidal drive: To become more certain about our findings for the $\epsilon = 0$ limit, we also study the effect of sinusoidal driving, where $J(t) = J \sin(2\pi t/T)$. We find that even for the sinusoidal drive protocol, the area-law entanglement phase sustains in the large L limit. Growth of trajectory averaged entanglement entropy for $T = 20$ and $\gamma = 0.05$ are shown in Fig. 11 for different L . We find that $L = 400$ and 550 data are almost indistinguishable, though for small L , the saturation values are different.

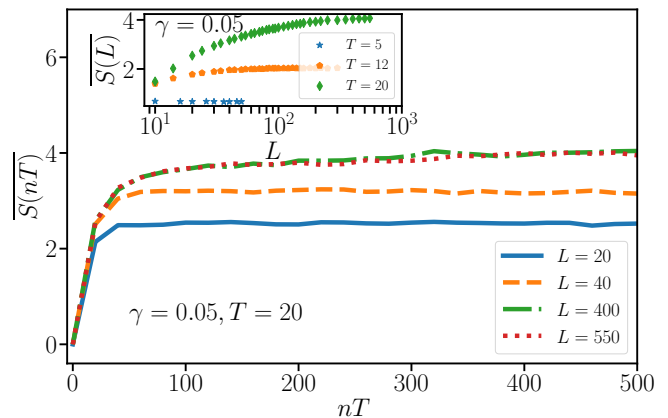


FIG. 11. Stroboscopic growth of trajectory averaged entanglement entropy for different L for the sinusoidal driving protocol for $T = 20$ and $\gamma = 0.05$ (main panel). Inset shows the system size scaling of the steady state trajectory averaged entanglement entropy for the different driving periods T . Data presented here are for $\gamma = 0.05$.

The inset of Fig. 11 shows the variation of the steady state entanglement entropy with L for different T , and it clearly shows the evidence of the area law in the large L limit, as already observed for the square pulse case. We also estimate the L_c using the fitting function $f(L)$ (see Eq. (16)) and compare it with square pulse results in Fig. 10 lower panel. We find that L_c is even smaller for sinusoidal drive compared to the square pulse.

V. CONCLUSIONS

In this work, we investigate the effect of periodic drive in a continuously monitored free-fermionic lattice model. It is well-known that in the absence of the drive, such systems undergo a measurement-induced entanglement phase transition from critical (logarithmic) to area law. Our main finding is that periodically driven non-interacting systems also go through a measurement-induced entanglement phase transition, and the universality class of this transition also seems to be preserved, which belongs to the BKT universality class. In general, for a given drive protocol, the low-frequency regime favors the critical phase more, implying that the critical measurement strength (transition point) increases with the time period. Moreover, we have also investigated a drive protocol in which the hopping amplitudes are varied completely symmetrically around zero in the form of square-pulse and sinusoidal drive and found that such a drive can't cause a phase transition independent of any frequency regime; it always promotes an area-law entanglement phase in the thermodynamic limit. This result is a bit surprising, especially given that disorder-induced similar-driven systems tend to favor de-localization in the low-frequency regime⁷⁵. Our results suggest several interesting directions for future work. The role of disorder

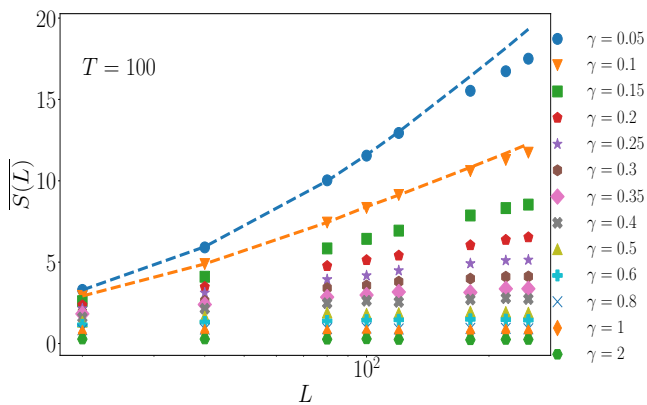


FIG. 12. Variation of steady state entanglement entropy with system size for different γ values for $T = 100$ for square pulse driving protocol with $\epsilon = 0$. The dashed lines show the no-drive ($J = 1/2$) results.

ders, interactions in the monitored Floquet system, and their relationship to Floquet-MBL¹⁰³ remain a challenging problem.

VI. ACKNOWLEDGEMENTS

R.M. acknowledges the DST-Inspire fellowship by the Department of Science and Technology, Government of India, SERB start-up grant (SRG/2021/002152). The authors also thank M Buchhold for fruitful discussions over private communication on the RG scheme. The authors also thank Xiangyu Cao for the fruitful discussion.

Appendix A: $T = 100$ result for square pulse protocol

Here, we discuss the $T = 100$ results. Dashed lines correspond to no-drive results for $J = 1/2$. It shows that almost up to $L \simeq 100$, the no-drive data is the same as the $T = 100$ data. Afterward, $T = 100$ data starts bending, while no-drive data keeps on increasing. In the main text, we show that in the case of square pulse protocol and a given driving time period T , for $L \gg L_c$, the steady state entanglement entropy does not change with L . The value of L_c was estimated using fitting function (16). It turns out that L_c increases exponentially with T , the fitted function predict the L_c to be 10^{16} for $T = 100$ and $\gamma = 0.05$. This suggests that due to our limitations of the accessible system size, we will be unable to identify the area-law phase for $\gamma = 0.05$ and $T = 100$. As expected, Fig. 12 shows no trace of area law for $\gamma = 0.05$. The data can mislead us to predict the usual BKT type critical to area law entanglement phase transition as we increase γ .

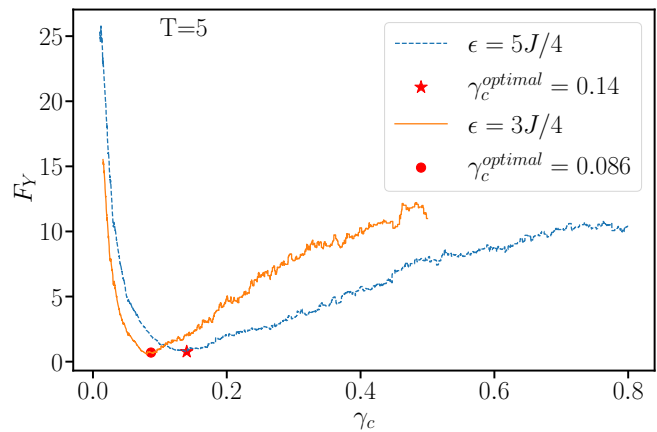


FIG. 13. Cost function F_Y vs. γ_c plot for different ϵ values. The star represents the optimal γ_c for $\epsilon = 5J/4$, and the circle represents the optimal γ_c value for $\epsilon = 3J/4$.

Appendix B: Cost-function minimization technique

In order to see the BKT transition, we had to perform a finite-size scaling analysis. The job is to find out the γ_c for which one can get the best possible data-collapse as observed in Fig. 7 (lower panel). We take $X_i = (\gamma - \gamma_c)(\ln L)^2$ for all the values of γ and L , and $Y_i = \overline{S(L, \gamma)} - \overline{S(L, \gamma_c)}$ sorted according to the increasing values of X_i . The values of $\overline{S(L, \gamma)}$, which are not in the list, have been calculated using linear extrapolation. Now, one can define the cost function as¹⁰⁴,

$$C_Y = \frac{\sum_{i=1}^P |Y_{i+1} - Y_i|}{\max\{Y_i\} - \min\{Y_i\}} - 1,$$

where P is the total number of unique X_i present in the list. For a perfect data-collapse, $C_Y = 0$. We perform a minimization of the function C_Y with respect to the free parameter γ_c and let for $\tilde{\gamma}_c$ the cost function is minimum, i.e., $C_Y(\tilde{\gamma}_c) = (C_Y)_{\min}$ (see Fig. 13). Usually, such minima in C_Y may not be that robust, by changing the input data set (adding or removing some data), minima can shift a bit. To incorporate that effect, we identify a set of $\{\gamma_c\}$ for which $C_Y \leq 2C_Y(\tilde{\gamma}_c)$. Then identify $\gamma_c^{(1)} = \min\{\gamma_c\}$ (minimum from that set) and $\gamma_c^{(2)} = \max\{\gamma_c\}$ (maximum from that set). We identify the optimal γ_c as $\gamma_c = (\gamma_c^{(1)} + \gamma_c^{(2)})/2$ (similar technique was used in Ref.⁴¹ to compute the error-bars).

Appendix C: F-test

We perform the F -test to quantitatively determine the statistical likelihood of our steady state entanglement data presenting a logarithmic scaling or volume law for small γ . The F -test is a likelihood-ratio test that assesses the goodness of fit of two competing statistical

models^{52,105}. For each set of $\overline{S(L)}$, we produce two curves \tilde{S}_L and $\tilde{S}_{\ln(L)}$, which are linear best-fits curves of $\overline{S(L)}$ in L and $\ln(L)$ respectively. These best-fit lines are used to compute the F_T -test statistic,

$$F_T = \frac{\tilde{E}_L}{\tilde{E}_{\ln(L)}}, \quad (\text{C1})$$

where \tilde{E}_L ($\tilde{E}_{\ln(L)}$) is the sum of the squared errors between $\overline{S(L)}$ and \tilde{S}_L ($\tilde{S}_{\ln(L)}$). The way F_T is constructed,

a lower F_T will favor volume law, and a higher F_T will favor logarithmic scaling. We exercise this test for our $\overline{S(L)}$ vs L data and found the $F_T \gg 1$ for $T = 5, 20, 100, 150, 200$ and for $\gamma = 0.05$, and $\epsilon = 3J/4$. It confirms that the scaling is most likely logarithmic.

* ph22d001@iittp.ac.in

† ranjan@iittp.ac.in

- ¹ Lev Vidmar and Marcos Rigol, “Entanglement entropy of eigenstates of quantum chaotic hamiltonians,” *Phys. Rev. Lett.* **119**, 220603 (2017).
- ² Lev Vidmar, Lucas Hackl, Eugenio Bianchi, and Marcos Rigol, “Entanglement entropy of eigenstates of quadratic fermionic hamiltonians,” *Phys. Rev. Lett.* **119**, 020601 (2017).
- ³ Lev Vidmar, Lucas Hackl, Eugenio Bianchi, and Marcos Rigol, “Volume law and quantum criticality in the entanglement entropy of excited eigenstates of the quantum ising model,” *Phys. Rev. Lett.* **121**, 220602 (2018).
- ⁴ Lucas Hackl, Lev Vidmar, Marcos Rigol, and Eugenio Bianchi, “Average eigenstate entanglement entropy of the xy chain in a transverse field and its universality for translationally invariant quadratic fermionic models,” *Phys. Rev. B* **99**, 075123 (2019).
- ⁵ Chaitanya Murthy and Mark Srednicki, “Structure of chaotic eigenstates and their entanglement entropy,” *Phys. Rev. E* **100**, 022131 (2019).
- ⁶ Tyler LeBlond, Krishnanand Mallayya, Lev Vidmar, and Marcos Rigol, “Entanglement and matrix elements of observables in interacting integrable systems,” *Phys. Rev. E* **100**, 062134 (2019).
- ⁷ Ranjan Modak and Tanay Nag, “Many-body dynamics in long-range hopping models in the presence of correlated and uncorrelated disorder,” *Phys. Rev. Res.* **2**, 012074 (2020).
- ⁸ Jens Eisert, Marcus Cramer, and Martin B Plenio, “Colloquium: Area laws for the entanglement entropy,” *Reviews of modern physics* **82**, 277–306 (2010).
- ⁹ Ranjan Modak and Bhabani Prasad Mandal, “Eigenstate entanglement entropy in a pt-invariant non-hermitian system,” *Physical Review A* **103**, 062416 (2021).
- ¹⁰ Rajibul Islam, Ruichao Ma, Philipp M Preiss, M Eric Tai, Alexander Lukin, Matthew Rispoli, and Markus Greiner, “Measuring entanglement entropy in a quantum many-body system,” *Nature* **528**, 77–83 (2015).
- ¹¹ Adam M Kaufman, M Eric Tai, Alexander Lukin, Matthew Rispoli, Robert Schittko, Philipp M Preiss, and Markus Greiner, “Quantum thermalization through entanglement in an isolated many-body system,” *Science* **353**, 794–800 (2016).
- ¹² Andreas Osterloh, Luigi Amico, Giuseppe Falci, and Rosario Fazio, “Scaling of entanglement close to a quantum phase transition,” *Nature* **416**, 608–610 (2002).
- ¹³ Pasquale Calabrese and John Cardy, “Entanglement entropy and quantum field theory,” *Journal of statistical mechanics: theory and experiment* **2004**, P06002 (2004).
- ¹⁴ Frank Pollmann, Subroto Mukerjee, Ari M Turner, and Joel E Moore, “Theory of finite-entanglement scaling at one-dimensional quantum critical points,” *Physical review letters* **102**, 255701 (2009).
- ¹⁵ Vincenzo Alba and Pasquale Calabrese, “Entanglement and thermodynamics after a quantum quench in integrable systems,” *Proceedings of the National Academy of Sciences* **114**, 7947–7951 (2017).
- ¹⁶ Shira Chapman, Jens Eisert, Lucas Hackl, Michal P Heller, Ro Jefferson, Hugo Marrochio, and Robert Myers, “Complexity and entanglement for thermofield double states,” *SciPost physics* **6**, 034 (2019).
- ¹⁷ Ranjan Modak, Vincenzo Alba, and Pasquale Calabrese, “Entanglement revivals as a probe of scrambling in finite quantum systems,” *Journal of Statistical Mechanics: Theory and Experiment* **2020**, 083110 (2020).
- ¹⁸ P. W. Anderson, “Absence of diffusion in certain random lattices,” *Phys. Rev.* **109**, 1492–1505 (1958).
- ¹⁹ D.M. Basko, I.L. Aleiner, and B.L. Altshuler, “Metal–insulator transition in a weakly interacting many-electron system with localized single-particle states,” *Annals of Physics* **321**, 1126–1205 (2006).
- ²⁰ Vadim Oganesyan and David A. Huse, “Localization of interacting fermions at high temperature,” *Phys. Rev. B* **75**, 155111 (2007).
- ²¹ Marko Žnidarič, Tomaž Prosen, and Peter Prelovšek, “Many-body localization in the heisenberg xxz magnet in a random field,” *Phys. Rev. B* **77**, 064426 (2008).
- ²² Arijeet Pal and David A. Huse, “Many-body localization phase transition,” *Phys. Rev. B* **82**, 174411 (2010).
- ²³ Maksym Serbyn, Z. Papić, and Dmitry A. Abanin, “Criterion for many-body localization-delocalization phase transition,” *Phys. Rev. X* **5**, 041047 (2015).
- ²⁴ Ranjan Modak and Subroto Mukerjee, “Many-body localization in the presence of a single-particle mobility edge,” *Phys. Rev. Lett.* **115**, 230401 (2015).
- ²⁵ Ming Gong, Gentil D. de Moraes Neto, Chen Zha, Yulin Wu, Hao Rong, Yangsen Ye, Shaowei Li, Qingling Zhu, Shiyu Wang, Youwei Zhao, Futian Liang, Jin Lin, Yu Xu, Cheng-Zhi Peng, Hui Deng, Abolfazl Bayat, Xiaobo Zhu, and Jian-Wei Pan, “Experimental characterization of the quantum many-body localization transition,” *Phys. Rev. Res.* **3**, 033043 (2021).
- ²⁶ Jens H. Bardarson, Frank Pollmann, and Joel E. Moore, “Unbounded growth of entanglement in models of many-

- body localization,” *Phys. Rev. Lett.* **109**, 017202 (2012).
- ²⁷ Jens H. Bardarson, Frank Pollmann, and Joel E. Moore, “Unbounded growth of entanglement in models of many-body localization,” *Phys. Rev. Lett.* **109**, 017202 (2012).
- ²⁸ Maksym Serbyn, Z. Papić, and Dmitry A. Abanin, “Universal slow growth of entanglement in interacting strongly disordered systems,” *Phys. Rev. Lett.* **110**, 260601 (2013).
- ²⁹ Yogeshwar Prasad and Arti Garg, “Initial state dependent dynamics across the many-body localization transition,” *Phys. Rev. B* **105**, 214202 (2022).
- ³⁰ Hyungwon Kim and David A. Huse, “Ballistic spreading of entanglement in a diffusive nonintegrable system,” *Phys. Rev. Lett.* **111**, 127205 (2013).
- ³¹ David J. Luitz, Nicolas Laflorencie, and Fabien Alet, “Many-body localization edge in the random-field heisenberg chain,” *Phys. Rev. B* **91**, 081103 (2015).
- ³² Ling-Na Wu and André Eckardt, “Bath-induced decay of stark many-body localization,” *Phys. Rev. Lett.* **123**, 030602 (2019).
- ³³ Henrik P. Lüschen, Pranjal Bordia, Sean S. Hodgman, Michael Schreiber, Saubhik Sarkar, Andrew J. Daley, Mark H. Fischer, Ehud Altman, Immanuel Bloch, and Ulrich Schneider, “Signatures of many-body localization in a controlled open quantum system,” *Phys. Rev. X* **7**, 011034 (2017).
- ³⁴ Emanuele Levi, Markus Heyl, Igor Lesanovsky, and Juan P. Garrahan, “Robustness of many-body localization in the presence of dissipation,” *Phys. Rev. Lett.* **116**, 237203 (2016).
- ³⁵ Mark H Fischer, Mykola Maksymenko, and Ehud Altman, “Dynamics of a many-body-localized system coupled to a bath,” *Phys. Rev. Lett.* **116**, 160401 (2016).
- ³⁶ Mariya V. Medvedyeva, Toma ž Prosen, and Marko Žnidarič, “Influence of dephasing on many-body localization,” *Phys. Rev. B* **93**, 094205 (2016).
- ³⁷ Ryusuke Hamazaki, Kohei Kawabata, and Masahito Ueda, “Non-hermitian many-body localization,” *Phys. Rev. Lett.* **123**, 090603 (2019).
- ³⁸ Jie Ren, Qiaoyi Li, Wei Li, Zi Cai, and Xiaoqun Wang, “Noise-driven universal dynamics towards an infinite temperature state,” *Phys. Rev. Lett.* **124**, 130602 (2020).
- ³⁹ Gonzalo Manzano Paule, “Thermodynamics and synchronization in open quantum systems,” (2018).
- ⁴⁰ O. Alberton, M. Buchhold, and S. Diehl, “Entanglement transition in a monitored free-fermion chain: From extended criticality to area law,” *Phys. Rev. Lett.* **126**, 170602 (2021).
- ⁴¹ Marcin Szyniszewski, Oliver Lunt, and Arijeet Pal, “Disordered monitored free fermions,” *Phys. Rev. B* **108**, 165126 (2023).
- ⁴² Xiangyu Cao, Antoine Tilloy, and Andrea De Luca, “Entanglement in a fermion chain under continuous monitoring,” *SciPost Physics* **7**, 024 (2019).
- ⁴³ Takaaki Minato, Koudai Sugimoto, Tomotaka Kuwahara, and Keiji Saito, “Fate of measurement-induced phase transition in long-range interactions,” *Phys. Rev. Lett.* **128**, 010603 (2022).
- ⁴⁴ T. Müller, S. Diehl, and M. Buchhold, “Measurement-induced dark state phase transitions in long-ranged fermion systems,” *Phys. Rev. Lett.* **128**, 010605 (2022).
- ⁴⁵ Kazuki Yamamoto and Ryusuke Hamazaki, “Localization properties in disordered quantum many-body dynamics under continuous measurement,” *Phys. Rev. B* **107**, L220201 (2023).
- ⁴⁶ Yohei Fuji and Yuto Ashida, “Measurement-induced quantum criticality under continuous monitoring,” *Phys. Rev. B* **102**, 054302 (2020).
- ⁴⁷ B. Ladewig, S. Diehl, and M. Buchhold, “Monitored open fermion dynamics: Exploring the interplay of measurement, decoherence, and free hamiltonian evolution,” *Phys. Rev. Res.* **4**, 033001 (2022).
- ⁴⁸ Jin Ming Koh, Shi-Ning Sun, Mario Motta, and Austin J Minnich, “Measurement-induced entanglement phase transition on a superconducting quantum processor with mid-circuit readout,” *Nature Physics* **19**, 1314–1319 (2023).
- ⁴⁹ M. Buchhold, Y. Minoguchi, A. Altland, and S. Diehl, “Effective theory for the measurement-induced phase transition of dirac fermions,” *Phys. Rev. X* **11**, 041004 (2021).
- ⁵⁰ Michele Fava, Lorenzo Piroli, Tobias Swann, Denis Bernard, and Adam Nahum, “Nonlinear sigma models for monitored dynamics of free fermions,” *Physical Review X* **13**, 041045 (2023).
- ⁵¹ Igor Poboiko, Paul Pöpperl, Igor V. Gornyi, and Alexander D. Mirlin, “Theory of free fermions under random projective measurements,” *Phys. Rev. X* **13**, 041046 (2023).
- ⁵² Bo Xing, Xhek Turkeshi, Marco Schiró, Rosario Fazio, and Dario Poletti, “Interactions and integrability in weakly monitored hamiltonian systems,” *Phys. Rev. B* **109**, L060302 (2024).
- ⁵³ A. Zabalo, M. J. Gullans, J. H. Wilson, R. Vasseur, A. W. W. Ludwig, S. Gopalakrishnan, David A. Huse, and J. H. Pixley, “Operator scaling dimensions and multifractality at measurement-induced transitions,” *Phys. Rev. Lett.* **128**, 050602 (2022).
- ⁵⁴ Piotr Sierant and Xhek Turkeshi, “Universal behavior beyond multifractality of wave functions at measurement-induced phase transitions,” *Phys. Rev. Lett.* **128**, 130605 (2022).
- ⁵⁵ Hisanori Oshima and Yohei Fuji, “Charge fluctuation and charge-resolved entanglement in a monitored quantum circuit with $u(1)$ symmetry,” *Phys. Rev. B* **107**, 014308 (2023).
- ⁵⁶ Zack Weinstein, Shane P. Kelly, Jamir Marino, and Ehud Altman, “Scrambling transition in a radiative random unitary circuit,” *Phys. Rev. Lett.* **131**, 220404 (2023).
- ⁵⁷ Jeremy Côté and Stefanos Kourtis, “Entanglement phase transition with spin glass criticality,” *Phys. Rev. Lett.* **128**, 240601 (2022).
- ⁵⁸ Maxwell Block, Yimu Bao, Soonwon Choi, Ehud Altman, and Norman Y. Yao, “Measurement-induced transition in long-range interacting quantum circuits,” *Phys. Rev. Lett.* **128**, 010604 (2022).
- ⁵⁹ Shengqi Sang and Timothy H. Hsieh, “Measurement-protected quantum phases,” *Phys. Rev. Res.* **3**, 023200 (2021).
- ⁶⁰ Oliver Lunt, Marcin Szyniszewski, and Arijeet Pal, “Measurement-induced criticality and entanglement clusters: A study of one-dimensional and two-dimensional clifford circuits,” *Phys. Rev. B* **104**, 155111 (2021).
- ⁶¹ Yaodong Li, Xiao Chen, Andreas W. W. Ludwig, and Matthew P. A. Fisher, “Conformal invariance and quantum nonlocality in critical hybrid circuits,” *Phys. Rev. B* **104**, 104305 (2021).
- ⁶² Ruihua Fan, Sagar Vijay, Ashvin Vishwanath, and Yi-Zhuang You, “Self-organized error correction in random unitary circuits with measurement,” *Phys. Rev. B* **103**,

- 174309 (2021).
- ⁶³ Aidan Zabalo, Michael J. Gullans, Justin H. Wilson, Sarang Gopalakrishnan, David A. Huse, and J. H. Pixley, “Critical properties of the measurement-induced transition in random quantum circuits,” *Phys. Rev. B* **101**, 060301 (2020).
- ⁶⁴ Xhek Turkeshi, Rosario Fazio, and Marcello Dalmonte, “Measurement-induced criticality in $(2 + 1)$ -dimensional hybrid quantum circuits,” *Phys. Rev. B* **102**, 014315 (2020).
- ⁶⁵ Michael J. Gullans and David A. Huse, “Scalable probes of measurement-induced criticality,” *Phys. Rev. Lett.* **125**, 070606 (2020).
- ⁶⁶ Michael J. Gullans and David A. Huse, “Dynamical purification phase transition induced by quantum measurements,” *Phys. Rev. X* **10**, 041020 (2020).
- ⁶⁷ Yimu Bao, Soonwon Choi, and Ehud Altman, “Theory of the phase transition in random unitary circuits with measurements,” *Phys. Rev. B* **101**, 104301 (2020).
- ⁶⁸ Soonwon Choi, Yimu Bao, Xiao-Liang Qi, and Ehud Altman, “Quantum error correction in scrambling dynamics and measurement-induced phase transition,” *Phys. Rev. Lett.* **125**, 030505 (2020).
- ⁶⁹ Qicheng Tang and W. Zhu, “Measurement-induced phase transition: A case study in the nonintegrable model by density-matrix renormalization group calculations,” *Phys. Rev. Res.* **2**, 013022 (2020).
- ⁷⁰ Chao-Ming Jian, Yi-Zhuang You, Romain Vasseur, and Andreas W. W. Ludwig, “Measurement-induced criticality in random quantum circuits,” *Phys. Rev. B* **101**, 104302 (2020).
- ⁷¹ K. Chahine and M. Buchhold, “Entanglement phases, localization, and multifractality of monitored free fermions in two dimensions,” *Phys. Rev. B* **110**, 054313 (2024).
- ⁷² Tony Jin and David G. Martin, “Measurement-induced phase transition in a single-body tight-binding model,” *Phys. Rev. B* **110**, L060202 (2024).
- ⁷³ Sibaram Ruidas and Sumilan Banerjee, “Semiclassical limit of a measurement-induced transition in many-body chaos in integrable and nonintegrable oscillator chains,” *Phys. Rev. Lett.* **132**, 030402 (2024).
- ⁷⁴ Tista Banerjee and K. Sengupta, “Entanglement transitions in a periodically driven non-hermitian ising chain,” *Phys. Rev. B* **109**, 094306 (2024).
- ⁷⁵ Madhumita Sarkar, Roopayan Ghosh, Arnab Sen, and K. Sengupta, “Mobility edge and multifractality in a periodically driven Aubry-André model,” *Phys. Rev. B* **103**, 184309 (2021).
- ⁷⁶ Madhumita Sarkar, Roopayan Ghosh, Arnab Sen, and K. Sengupta, “Signatures of multifractality in a periodically driven interacting Aubry-André model,” *Phys. Rev. B* **105**, 024301 (2022).
- ⁷⁷ Tanay Nag, Sthitadhi Roy, Amit Dutta, and Diptiman Sen, “Dynamical localization in a chain of hard core bosons under periodic driving,” *Phys. Rev. B* **89**, 165425 (2014).
- ⁷⁸ Adhip Agarwala, Utso Bhattacharya, Amit Dutta, and Diptiman Sen, “Effects of periodic kicking on dispersion and wave packet dynamics in graphene,” *Phys. Rev. B* **93**, 174301 (2016).
- ⁷⁹ David J. Luitz, Achilleas Lazarides, and Yevgeny Bar Lev, “Periodic and quasiperiodic revivals in periodically driven interacting quantum systems,” *Phys. Rev. B* **97**, 020303 (2018).
- ⁸⁰ Vedika Khemani, Achilleas Lazarides, Roderich Moessner, and S. L. Sondhi, “Phase structure of driven quantum systems,” *Phys. Rev. Lett.* **116**, 250401 (2016).
- ⁸¹ Dominic V. Else, Bela Bauer, and Chetan Nayak, “Floquet time crystals,” *Phys. Rev. Lett.* **117**, 090402 (2016).
- ⁸² Jiehang Zhang, Paul W Hess, A Kyrianiadis, Petra Becker, A Lee, J Smith, Gaetano Pagano, I-D Potirniche, Andrew C Potter, Ashvin Vishwanath, et al., “Observation of a discrete time crystal,” *Nature* **543**, 217–220 (2017).
- ⁸³ Takashi Oka and Hideo Aoki, “Photovoltaic hall effect in graphene,” *Phys. Rev. B* **79**, 081406 (2009).
- ⁸⁴ Netanel H Lindner, Gil Refael, and Victor Galitski, “Floquet topological insulator in semiconductor quantum wells,” *Nature Physics* **7**, 490–495 (2011).
- ⁸⁵ Takuya Kitagawa, Takashi Oka, Arne Brataas, Liang Fu, and Eugene Demler, “Transport properties of nonequilibrium systems under the application of light: Photoinduced quantum hall insulators without Landau levels,” *Phys. Rev. B* **84**, 235108 (2011).
- ⁸⁶ Arijit Kundu, H. A. Fertig, and Babak Seradjeh, “Effective theory of Floquet topological transitions,” *Phys. Rev. Lett.* **113**, 236803 (2014).
- ⁸⁷ Bhaskar Mukherjee, Arnab Sen, Diptiman Sen, and K. Sengupta, “Signatures and conditions for phase band crossings in periodically driven integrable systems,” *Phys. Rev. B* **94**, 155122 (2016).
- ⁸⁸ Achilleas Lazarides, Arnab Das, and Roderich Moessner, “Fate of many-body localization under periodic driving,” *Phys. Rev. Lett.* **115**, 030402 (2015).
- ⁸⁹ Pedro Ponte, Z. Papić, François Huveneers, and Dmitry A. Abanin, “Many-body localization in periodically driven systems,” *Phys. Rev. Lett.* **114**, 140401 (2015).
- ⁹⁰ Stefano Scopa, Gabriel T. Landi, Adam Hammoumi, and Dragi Karevski, “Exact solution of time-dependent Lindblad equations with closed algebras,” *Phys. Rev. A* **99**, 022105 (2019).
- ⁹¹ Tatsuhiko N. Ikeda, Koki Chinzei, and Masahiro Sato, “Nonequilibrium steady states in the Floquet-Lindblad systems: van Vleck’s high-frequency expansion approach,” *SciPost Phys. Core* **4**, 033 (2021).
- ⁹² H. M. Wiseman and G. J. Milburn, “Quantum theory of field-quadrature measurements,” *Phys. Rev. A* **47**, 642–662 (1993).
- ⁹³ Bernt Øksendal and Bernt Øksendal, “Stochastic differential equations,” (2003).
- ⁹⁴ Brian Skinner, Jonathan Ruhman, and Adam Nahum, “Measurement-induced phase transitions in the dynamics of entanglement,” *Physical Review X* **9**, 031009 (2019).
- ⁹⁵ Takaaki Minato, Koudai Sugimoto, Tomotaka Kuwahara, and Keiji Saito, “Fate of measurement-induced phase transition in long-range interactions,” *Physical review letters* **128**, 010603 (2022).
- ⁹⁶ Luigi Amico, Rosario Fazio, Andreas Osterloh, and Vlatko Vedral, “Entanglement in many-body systems,” *Rev. Mod. Phys.* **80**, 517–576 (2008).
- ⁹⁷ Ingo Peschel, “Calculation of reduced density matrices from correlation functions,” *Journal of Physics A: Mathematical and General* **36**, L205 (2003).
- ⁹⁸ Ingo Peschel and Viktor Eisler, “Reduced density matrices and entanglement entropy in free lattice models,” *Journal of physics a: mathematical and theoretical* **42**, 504003 (2009).

- ⁹⁹ Horacio Casini and Marina Huerta, “Entanglement entropy in free quantum field theory,” *Journal of Physics A: Mathematical and Theoretical* **42**, 504007 (2009).
- ¹⁰⁰ Marin Bukov, Luca D’Alessio, and Anatoli Polkovnikov, “Universal high-frequency behavior of periodically driven systems: from dynamical stabilization to floquet engineering,” *Advances in Physics* **64**, 139–226 (2015).
- ¹⁰¹ Daniel J Amit, Yadin Y Goldschmidt, and S Grinstein, “Renormalisation group analysis of the phase transition in the 2d coulomb gas, sine-gordon theory and xy-model,” *Journal of Physics A: Mathematical and General* **13**, 585 (1980).
- ¹⁰² Kenji Harada and Naoki Kawashima, “Universal jump in the helicity modulus of the two-dimensional quantum xy model,” *Physical Review B* **55**, R11949 (1997).
- ¹⁰³ Piotr Sierant, Maciej Lewenstein, Antonello Scardicchio, and Jakub Zakrzewski, “Stability of many-body localization in floquet systems,” *Phys. Rev. B* **107**, 115132 (2023).
- ¹⁰⁴ Jan Šuntajs, Janez Bonča, Tomaž Prosen, and Lev Vidmar, “Ergodicity breaking transition in finite disordered spin chains,” *Phys. Rev. B* **102**, 064207 (2020).
- ¹⁰⁵ Alexander McFarlane Mood, “Introduction to the theory of statistics.” (1950).